Development/Plasticity/Repair

Control of G_2 Phase Duration by CDC25B Modulates the Switch from Direct to Indirect Neurogenesis in the Neocortex

Melanie Roussat, Thomas Jungas, Christophe Audouard, Sofiane Omerani, Francois Medevielle, Eric Agius, Alice Davy, Fabienne Pituello, and Sophie Bel-Vialar

Molecular, Cellular and Developmental biology unit (UMR 5077), Center for Integrative Biology, Université Paul Sabatier, Toulouse, cedex 09, France

During development, cortical neurons are produced in a temporally regulated sequence from apical progenitors, directly or indirectly, through the production of intermediate basal progenitors. The balance between these major progenitor types is critical for the production of the proper number and types of neurons, and it is thus important to decipher the cellular and molecular cues controlling this equilibrium. Here we address the role of a cell cycle regulator, the CDC25B phosphatase, in this process. We show that, in the developing mouse neocortex of both sex, deleting CDC25B in apical progenitors leads to a transient increase in the production of $TBR1^+$ neurons at the expense of $TBR2^+$ basal progenitors. This phenotype is associated with lengthening of the G_2 phase of the cell cycle, the total cell cycle length being unaffected. Using *in utero* electroporation and cortical slice cultures, we demonstrate that the defect in $TBR2^+$ basal progenitor production requires interaction with CDK1 and is because of the G_2 phase lengthening in CDC25B mutants. Together, this study identifies a new role for CDC25B and G_2 phase length in direct versus indirect neurogenesis at early stages of cortical development.

Key words: **CDC25B; cell cycle; differentiation; neocortex; neural stem cells; neurogenesis**

Significance Statement

This study is the first analysis of the function of CDC25B, a G_2/M regulator, in the developing neocortex. We show that removing CDC25B function leads to a transient increase in neuronal differentiation at early stages, occurring simultaneously with a decrease in basal intermediate progenitors (bIPs). Conversely, a CDC25B gain of function promotes production of bIPs, and this is directly related to CDC25B's ability to regulate CDK1 activity. This imbalance of neuron/progenitor production is linked to a G_2 phase lengthening in apical progenitors; and using pharmacological treatments on cortical slice cultures, we show that shortening the G_2 phase is sufficient to enhance bIP production. Our results reveal the importance of G_2 phase length regulation for neural progenitor fate determination.

Introduction

During mammalian brain development, neural progenitor cells (NPCs) undergo precise sequential transitions that will define the number and type of neurons that will compose the neocortex (Kawaguchi, 2019). It is therefore important that the proliferation and differentiation rates of these progenitors be tightly regulated during neurogenesis, to avoid dramatic cortical defects, such as microcephaly in humans (Barbelanne and Tsang, 2014).

At the onset of corticogenesis, NPCs initially divide symmetrically to expand the stem cell pool, before giving rise to apical dividing progenitors (Govindan and Jabaudon, 2017). Apical radial glial cells (aRGs) first divide symmetrically and then shift to an asymmetric self-renewing division, producing an aRG and either a neuron (direct neurogenesis) or a basal intermediate progenitor (bIP), that divide once to produce two neurons (indirect neurogenesis) (Govindan and Jabaudon, 2017; Kawaguchi, 2019). Another type of basal progenitor, basal radial glia (bRG, also called outer radial glia), has emerged during evolution and is also present in very small proportions in the subventricular zone (SVZ) and intermediate zone of rodents (Namba and Huttner, 2017; Ostrem et al. 2017). All these progenitors produce sequentially the different types of

Received Apr. 29, 2022; revised Nov. 15, 2022; accepted Nov. 23, 2022.

Author contributions: M.R. and S.B.-V. designed research; M.R., T.J., C.A., S.O., F.M., and S.B.-V. performed research; M.R. and S.B.-V. analyzed data; M.R., A.D., F.P., and S.B.-V. edited the paper; E.A., A.D., and F.P. contributed unpublished reagents/analytic tools; S.B.-V. wrote the paper.

Work in F.P.'s laboratory was supported by Center National de la Recherche Scientifique, Université P. Sabatier, and Agence Nationale de la Recherche ANR-19-CE16-0006-01. M.R. was supported by Ministère de L'Enseignement Supérieur et de la Recherche. We thank Valerie Lobjois for fruitful discussions; and Myriam Roussigné, Elise Cau, and Mohamad Fawal for critical reading of the manuscript.

The authors declare no competing financial interests.

Correspondence should be addressed to Sophie Bel-Vialar at sophie.vialar@univ-tlse3.fr.

https://doi.org/10.1523/JNEUROSCI.0825-22.2022

projection neurons that colonize the six layers of the adult neocortex (Kawaguchi, 2019). The temporal transitions from one type of progenitor to another are therefore key parameters in controlling the size and functionality of the adult neocortex (Wilsch-Bräuninger et al., 2016).

Cell cycle kinetics, and in particular cell cycle phase duration, is of major importance for controlling these transitions (Dehay and Kennedy, 2007; Agius et al., 2015). Several studies showed that G_1 lengthening is an important positive regulator of neuronal differentiation, G_1 phase lengthening being associated with the transition from aRGs to bIPs during corticogenesis (Lange et al., 2009; Pilaz et al., 2009; Arai et al., 2011). In addition, it has been shown that proliferating and neurogenic progenitors display different S phase duration, the latter having a shorter S phase (Arai et al., 2011). Mitosis lengthening is also linked to an increase in neurogenic divisions (Pilaz et al., 2016). However, even if correlations have been made in different organs between the duration of G_2 phase and cell fate (Locker et al., 2006; Agathocleous et al., 2007; Gonzales and Liang, 2015; Gonzales et al., 2015), the importance of controlling G_2 length during neurogenesis remains poorly documented.

A few years ago, we showed that the CDC25B phosphatase, a master regulator of mitosis entry, favors neurogenic division at the expense of proliferative ones, and that part of this function is independent of its interaction with CDK1 (Benazeraf et al., 2006; Peco et al., 2012; Bonnet et al., 2018). CDC25B is a well-known G_2/M regulator, belonging to the dual specificity CDC25 phosphatase family that activates CDK1-cyclinB complexes and thus promotes mitosis entry (Boutros et al., 2007). It is also recruited to the mother centrosome and is involved in the centrosome duplication cycle, as well as in microtubule nucleation (Boutros et al., 2007, 2011, 2013; Boutros and Ducommun, 2008). Our previous work shows that it allows progenitor maturation in the developing spinal cord, but it remains an open question whether this phosphatase can be considered a general player in neuronal maturation and whether regulation of G_2 phase duration has a role to play in this process.

In this study, we investigate the role of CDC25B in corticogenesis. Using a conditional CDC25B KO mouse line, we show that CDC25B loss of function in apical progenitors leads to a transient imbalance in neuronal and bIP production, accompanied by a significant lengthening of the G_2 phase. We provide evidence that this change in G_2 duration in apical progenitors causes the switch in fate, producing neurons instead of bIPs. This study sheds light on an important role of CDC25B and G_2 phase modulation for controlling the fate of apical progenitors, thus impacting the switch between direct to indirect neurogenesis.

Materials and Methods

Mice. Experiments were performed in accordance with European Community guidelines regarding care and use of animals, in agreement with the Ministère de l'Enseignement Supérieur et de la Recherche (number C3155511, reference 01024.01) and CNRS recommendations. *Cdc25b*$^{+/-}$; Nestin-Cre, and Cdc25b$^{flox/flox}$ lines have been described previously (Tronche et al., 1999; Bonnet et al., 2018). These lines were crossed to obtain conditional mutant embryos Cdc25$^{flox/-}$; nestin-Cre (cKO) and control embryos Cdc25b$^{flox/-}$, Cdc25b$^{flox/+}$ and *Cdc25b flox/*$^{+}$; nestin-Cre (Control) of either sex. *Tis21-GFP* line (*Tis21*$^{-/tm2(Gfp)Wb}$) has been described previously (Haubensak et al., 2004). This line was crossed to obtain conditional mutant embryos Cdc25b$^{flox/-}$; nestin-Cre; *Tis21-GFP* that express GFP under the control of the Tis21 promotor. Embryonic (E) day 0.5 was assumed to start at midday of the day of the vaginal plug.

Table 1. Cell cycle parameters in Ctl and cKO aRGs

E14.5	T_C	T_S	T_{G2}	$^*T_{G1}$
Control	17 h 58	4 h 47	2 h 12	10 h 29
Cdc25b^{nesKO}	18 h 15	4 h 41	4 h 05	8 h 59
ΔT	0 h 18	−0 h 06	1 h 53	−1 h 30
%FC	1.7%	−2%	85%	−14%

ISH and immunohistochemistry. ISH was performed on 60 µm vibratome coronal sections of mouse brain embryos as described previously (Bonnet et al., 2018). For immunohistochemistry, embryos were fixed in 4% PFA at 4°C overnight, washed in PBS, and embedded in paraffin using an STP 120 Spin Tissue Processor. Brains were sliced in 6-14 µm transversal sections using a HM 355 Microtom. Sections were directly mounted on coated histologic slides. Sections were rehydrated in successive baths of histoclear (twice), 100% ethanol (twice), 95% ethanol, 70% ethanol, 50% ethanol, and deionized H_20 for 5 min each. Sections were heated in 1% citrate in H_2O at ~100°C for 45 min, permeabilized with PBS-0.5% Tween + 3% BSA + 1% horse serum and incubated with primary antibody overnight at 4°C. The following primary antibodies were used against: P-H3 (Millipore Biotechnology, 1:1000, rabbit), BrdU (G3G4, 1:400, mouse), active caspase 3 (BD Biosciences, 1:100, rabbit), GFP (Abcam, 1:1000, chick), CCND1 (Fisher Scientific, 1:200, rabbit), SATB2 (Abcam, 1:100, mouse), TBR1 (Abcam, 1:100, rabbit), PAX6 (Covance, 1:300, rabbit), PAX6 (MBL; 1:200, rabbit), TBR2 (eBioscience, 1:50, rat), RFP (SICGEN, 1:100, goat), CTIP2 (Abcam, 1:200, rat), and CUX1 (Santa Cruz Biotechnology, 1:100). Sections were then washed in PBS and incubated with secondary antibodies for 2 h at room temperature. We counterstained the sections with DAPI (1:1000, Invitrogen) to identify nuclei. For BrdU detection, we treated sections with 2N HCl and then with 0.1 M $Na_4B_4O_7$ before incubation with primary antibodies.

Cell proliferation, cell cycle, and birth dating analysis/5-ethynyl-2′-deoxyuridine (EdU)/BrdU experiments. We determined G_2 phase length using the percentage of labeled mitoses (PLM) paradigm (Quastler and Sherman, 1959). We injected pregnant mice intraperitoneally with 100 µl of EdU (Click-iT EdU AlexaFluor-647 Imaging Kit, Invitrogen) at 1 mg/ml. Embryos were harvested 120, 180, 240, 300, 360, or 480 min after EdU administration, and we quantified the percentage of P-H3$^+$EdU$^+$ colabeled nuclei with increasing times of exposure to EdU. The progression of this percentage is proportional to G_2 phase duration. To determine cell proliferation, we injected pregnant mice intraperitoneally with 1 mg/ml of EdU. Embryos were harvested 60 min later. Total cell cycle length and S phase length were determined as described previously (Martynoga et al., 2005). We injected pregnant mice intraperitoneally with 100 µl of EdU 10 mg/ml, followed by 100 µl of BrdU (Sigma) at 10 mg/ml 90 min later. Embryos were collected 30 min later. We calculated Tc and Ts from counts of EdU$^+$BrdU$^-$ and EdU$^+$BrdU$^+$ cells. To determine generation of neurons by pulse-chase experiments (birth dating), we injected pregnant mice intraperitoneally with EdU at E16.5, and we harvested embryos at birth (P0). We deduced G_1 phase length by removing the average length of G_2 + S + M phases from the average total cell cycle length in control and *CDC25B*^{cKO} littermates.

Flow cytometry analysis. Flow cytometry analysis was conducted as described by Jungas et al. (2020). Cortical hemispheres were collected in PBS-1% FCS and cells mechanically dissociated through a 40 µm nylon mesh (Clearline). We suspended cells in 1.2 ml ice-cold PBS and fixed them by slowly adding 3 ml cold 100% ethanol while vortexing to obtain a 70% final concentration. The incubation procedure with primary and secondary antibodies was as described for immunofluorescence, with centrifugation at 2200 rpm for 10 min at each step. Finally, cells were resuspended in 500 µl PI/RNase solution for 30 min in the dark. Acquisition was performed using cytoflexS with a minimum of 1000 cells with the Cytexpert software. We excluded debris and doublets using morphometric parameters (FSC/SSC) and pulse area parameters from PI emission, respectively. To set the threshold of PAX6-, TBR2-, CTIP2-, SATB2-, and GFP-positive cells, control samples cells were incubated with secondary antibody and PI only.

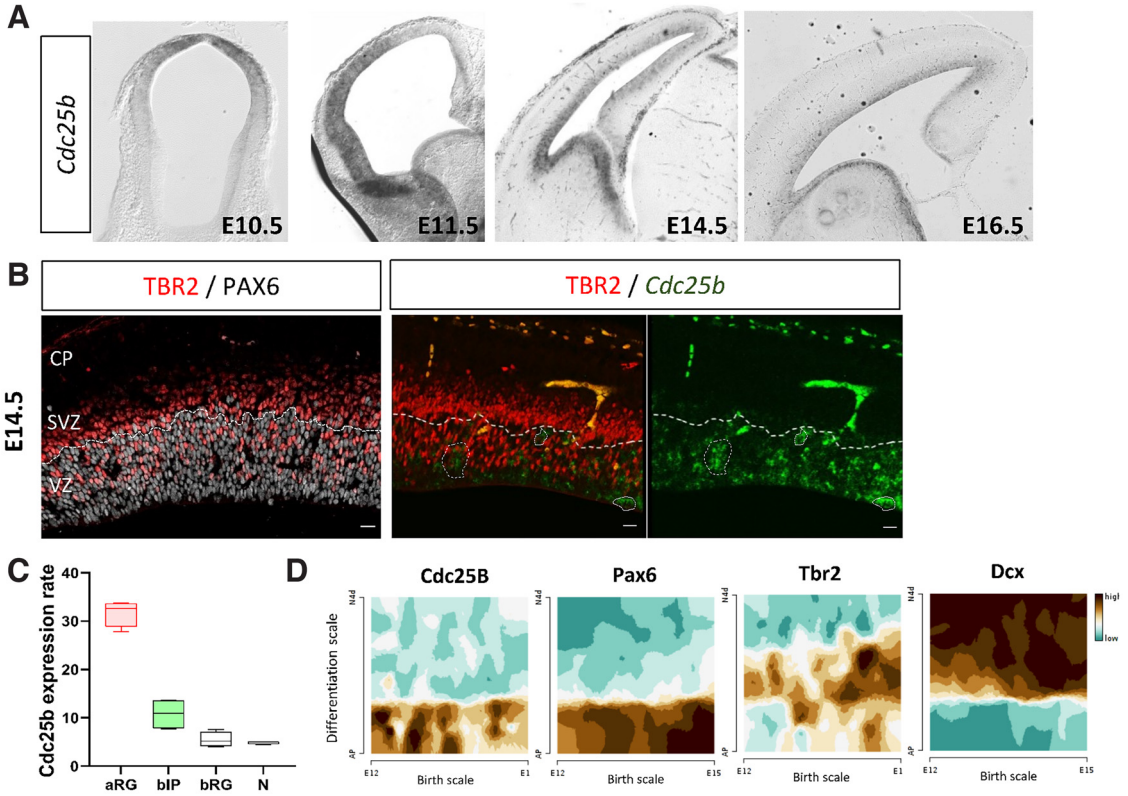

Figure 1. *Cdc25B* expression pattern during corticogenesis. *Cdc25B* is expressed in aRG progenitors ($PAX6^+$ in the VZ) and progressively downregulated in basal progenitors ($TBR2^+$). ***A***, *Cdc25B* ISH on mouse embryo coronal sections at E10.5, E11.5, E14.5, and E16.5. ***B***, PAX6 and TBR2 immunostaining and costaining of *Cdc25b* (ISH) and TBR2 expression (immunofluorescence) on E14.5 coronal brain sections. ***C***, ***D***, Quantification of *CDC25B* transcripts in progenitors and neurons using bulk RNA-Seq data from Florio et al. (2015) (***C***) and single-cell RNA-Seq from Telley et al. (2019) using the gene browser at http://genebrowser.unige.ch/telagirdon/ (***D***).

aRG progenitor DNA content was estimated by analyzing PI emission intensity of PAX6-positive cells only.

Organotypic brain slice culture and drug treatment. Coronal slices of E13.5 control and $CDC25B^{cKO}$ embryos were sectioned at 250 µm on a vibratome (Leica Microsystems). We deposited coronal slices on Millicell Cell Culture insert (0.4 µm, Millipore) in culture medium DMEM-F12, 1× penicilin/streptavidin. Slices remained incubated in 5% CO_2 at 38°C for 24 h. For drug treatment, brain slices were incubated in culture medium containing 1 μM PD0166285 (Selleckchem).

To determine cell proliferation and the PLM paradigm, 250 μM EdU was dropped off directly on each slice, for the duration required, depending on the analysis (see above cell proliferation section). Brain slices were fixed 1 h at room temperature in 4% PFA, and sectioned at 60 µm with a vibratome before immunostaining.

DNA constructs and in utero *electroporation. In utero* electroporation experiments were performed in cortices of E13.5 embryos inside the pregnant mother as described previously (Fawal et al., 2018) . Embryos were harvested 28 h later. Gain-of-function experiments were performed using a vector expressing two human *Cdc25B* forms, hCDC25B3 (*Cdc25B* WT) or hCDC25B3delCDK (*Cdc25B*delCDK), under the control of a *cis* regulatory element of the mouse *Cdc25B* called pccRE (Körner et al., 2001; Bonnet et al., 2018). A control vector was generated with the β-Gal gene downstream of the pccRE; 1.5 mg/ml of either plasmid expressing *Cdc25b* or control plasmid was coinjected with 1 µg/µl pCIG-GFP and Fast Green (Sigma) in the lateral ventricle of embryos neocortex, manually using a beveled and calibrated glass micropipette. For electroporation, five 50 ms pulses of 35 V with a 950 ms interval were delivered across the uterus with two 3 mm electrode paddles positioned on either side of the head. Before surgery, mice were subcutaneously injected with 100 µl of morphine at 2.5 mg/kg. Mice were anesthetized with 4% isoflurane. After surgery, mice were subcutaneously injected with 100 µl of 2 mg/ml metacam.

Imaging and statistical analysis. All images of immunostained sections were acquired using a SP8 Leica confocal microscope. For each experiment, we analyzed at least three independent litters and three different slides per embryo. The quantifications were performed in the lateral half of the intermediary cortex, except for the G_2 length estimation, for which the P-H3/EdU count was performed in the entire hemisection. For each experiment, we verified that the cell density was the same between Ctl and cKO. Quantitative data are expressed as mean ± SEM. They are represented as scatter plots with a bar, each point showing the value for one embryo, or as a violin plot, when the number of measures was large enough (see Fig. 5). Table 1 was established from the values reported in Figure 6. Statistical analyses were performed using Graph Pad Prism 9 or the RStudio software. Significance was assessed by performing the Mann–Whitney *t* test, the Wilcoxon test, or using the mixed effect model followed by an ANOVA test as described previously (Bonnet et al., 2018).

Results

Cdc25b is expressed in apical progenitors

To determine whether *Cdc25b* is expressed in all cortical progenitors or in a subset of them, we performed ISH on brain coronal sections at key stages of corticogenesis (Fig. 1*A*). *Cdc25b* is detected in neuroepithelial cells from E10.5. At E11.5, *Cdc25b* is expressed in the ventricular zone (VZ) of the cortex, consisting of proliferating progenitors. At E14.5 and E16.5, it still appears restricted to the VZ that contains $PAX6^+$ apical progenitors (aRGs) and $TBR2^+$ newborn basal progenitors (bIPs) (Fig. 1*A*). To determine whether it is also expressed in the SVZ, we performed immunostaining for TBR2 following ISH of *Cdc25b* transcripts at E14.5. We observed that *Cdc25b* is not expressed in the SVZ, which contains $TBR2^+$ bIPs, and that the $TBR2^+$ cells in the VZ (newborn bIPs) (Arai et al., 2011) do not overlap with *Cdc25b*-

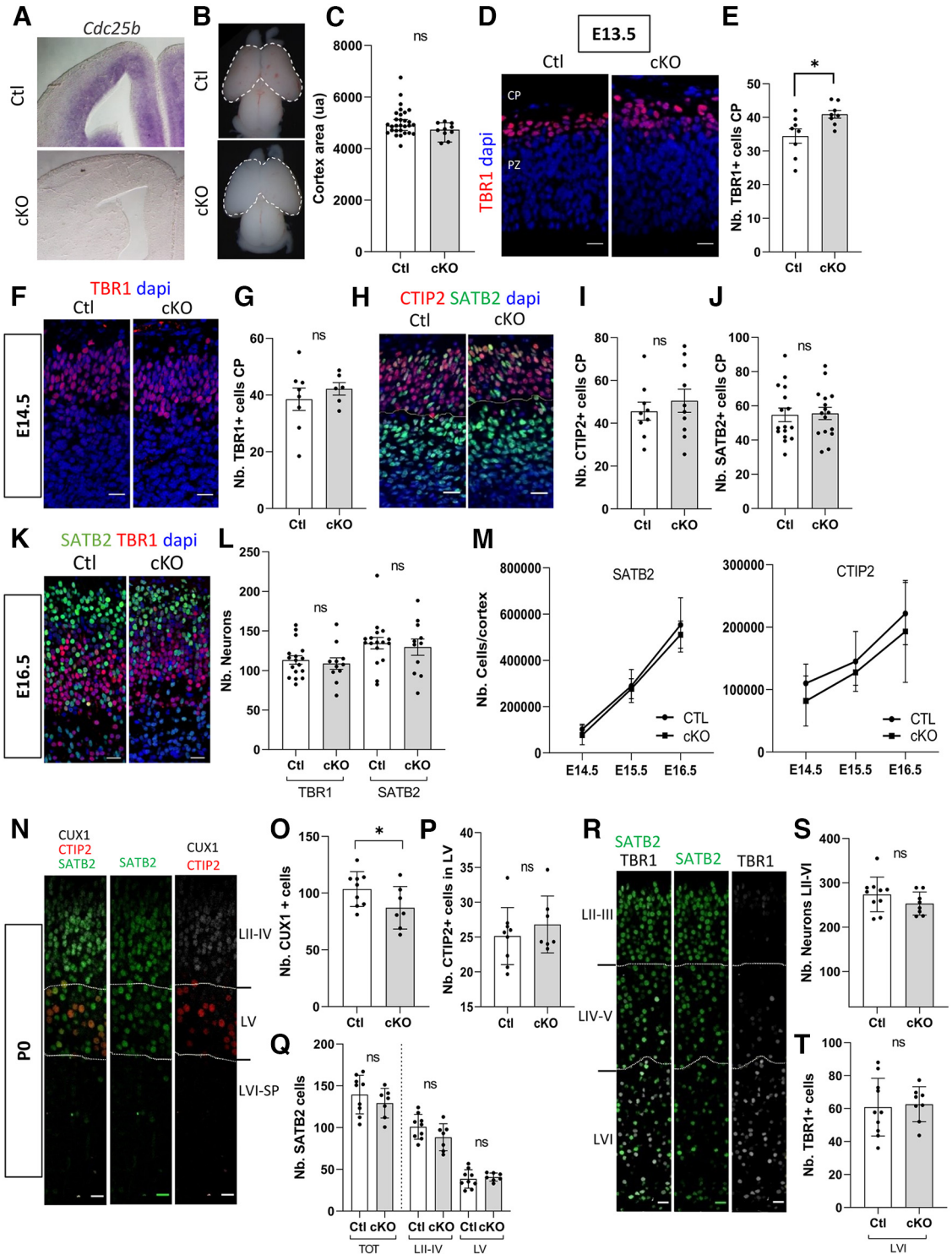

Figure 2. *Cdc25B* loss of function triggers a transient increase of neuronal differentiation and a defect of neuronal specification. ***A***, *Cdc25B* ISH at E14.5 on control (Ctl) and *Cdc25b* cKO embryo coronal sections. ***B***, ***C***, Cortical area (white dotted line) measurement in Ctl and cKO embryos at P0. ***C***, Each point represents the cortex area in arbitrary unit (ua) for one embryo. Mann–Whitney *t* test and mixed model. Ctl, $n = 29$; cKO, $n = 10$. ***D***, ***F***, TBR1 immunostaining on coronal sections at E13.5 (***D***) and E14.5 (***F***). Nuclei are stained with DAPI (blue nuclei). ***E***, ***G***, Quantification of TBR1 neurons in the cortical plate (red nuclei) at E13.5 and E14.5. Each point is the mean value of 3 sections/embryo. Mixed model. E13.5, $n = 9$ or 10. $^*p = 0.019$. E14.5, $n = 6$–8. ***H–J***, Quantification of CTIP2 (***I***) and SATB2 neurons (***J***) in the cortical plate at E14.5. Each point is the mean value of 3 sections/embryo. Mixed model. CTIP2, $n = 9$ or 10; SATB2, $n = 16$. ***K***, TBR1 (red nuclei) and SATB2 (green nuclei) immunostaining on coronal sections at E16.5; nuclei are stained with DAPI (blue nuclei). ***L***, Quantification of $SATB2^+$ and $TBR1^+$ neurons in Ctl and cKO embryos at E16.5. Each point is the mean value of 3 sections/embryo. Ctl, $n = 17$; cKO, $n = 11$. Mixed model. ***M***, Dynamics of neuronal production in Ctl and cKO quantified by FACS of SATB2 and CTIP2 neurons from E14.5 to E16.5. Each point represents the mean number of cells of several cortices: E14.5, Ctl, $n = 6$; cKO, $n = 5$; E15.5, Ctl, $n = 6$; cKO, $n = 3$; E16.5, Ctl, $n = 6$; cKO, $n = 2$. ***N***, CUX1, CTIP2, and SATB2 immunostaining on P0 coronal brain sections of Ctl embryos. ***O–Q***, Quantification of CUX1 (***O***), CTIP2 (***P***), and SATB2 (***Q***) cells in Ctl and cKO embryos at P0. Ctl, $n = 9$; cKO, $n = 7$. Mixed model. $^*p = 0.043$. Each point is the mean value of 3 sections/embryo. ***R***, TBR1 (gray nuclei) and SATB2 (green nuclei) immunostaining on coronal sections at P0. ***S***, Total number of neurons in layers II-VI (SATB2+TBR1 neurons) at P0 in 100 μm wide on coronal sections from ***R***. ***T***, Quantification of $TBR1^+$ neurons in layer VI in 100 μm wide on coronal sections from ***R***. Each point represents the mean value of 3 sections/embryo. Ctl, $n = 10$; cKO, $n = 8$, Mixed model. CP, Cortical plate; PZ, progenitor zone. Scale bars, 20 μm.

expressing cells either (Fig. 1*B*). To confirm this observation, we analyzed published bulk RNA-Seq data from E14.5 samples (Florio et al., 2015) and scRNA-Seq data from E12 to E15 cortices (Telley et al., 2019). This data mining confirmed that *Cdc25b* is highly expressed in aRGs, barely in bIPs, and is not expressed in bRGs and neurons (Fig. 1*C*,*D*). Overall, these analyses indicate that, in the developing cortex, *Cdc25b* is predominantly expressed in aRGs, progressively extinguished in bIPs, and absent in neurons.

Cdc25b deletion transiently leads to increased neuronal differentiation and decreased basal progenitor production

Having determined that *Cdc25b* expression is restricted to the apical progenitors, we next investigated its function during the early phases of corticogenesis in *Cdc25bfl/-*; *NestinCre* (*Cdc25b*^{cKO} or cKO) embryos, in which *Cdc25b* expression is specifically extinguished in NPCs from the onset of neurogenesis (Bonnet et al., 2018). In these embryos, deletion is complete in the cortex from E10.5 (Madisen et al., 2010); and at E14.5, *Cdc25b* expression is abolished in the whole brain (Fig. 2*A*). We first measured cortical hemisphere size at the postnatal stage (P0) and did not observe any gross size defect in *Cdc25b*^{cKO} newborns (Fig. 2*B*,*C*). We then checked the production of different types of neurons over time. TBR1-, CTIP2-, and SATB2-expressing neurons are sequentially produced between E12.5 and E16.5 (Molyneaux et al., 2007; Vasistha et al., 2015). At E13.5, the majority of neurons express TBR1. In *Cdc25b*^{cKO}, the number of TBR1$^+$ neurons is transiently increased in the most lateral part of the cortical plate at E13.5 (Fig. 2*D*,*E*). This increase is no longer significant at E14.5 (Fig. 2*F*,*G*). We then checked CTIP2$^+$ and SATB2$^+$ neurons at E14.5 and found that their production occurs normally at this stage in *Cdc25b*^{cKO} (Fig. 2*H*–*J*). At E15.5 and E16.5, no difference is observed in the number of TBR1$^+$, CTIP2$^+$, or SATB2$^+$ neurons (Fig. 2*K*–*M*). These results indicate that, in *Cdc25b*^{cKO}, neuronal production is transiently increased at E13.5 but has returned to normal at later stages.

To examine whether this transient increase of neuron production at E13.5 induces a change in neuron specification, we quantified the number of neurons in several layers at P0 using CTIP2 (layer V), SATB2, CUX1 (LII-III), and TBR1 (LVI) (Fig. 2*N*–*T*). Only the CUX1$^+$ neuron number was slightly reduced in layers II-III (Fig. 2*O*). As CUX1$^+$ neurons are mainly produced from TBR2$^+$ basal progenitors (Vasistha et al., 2015), this suggests that, in cKO, the increased production of TBR1 neurons at E13.5 is made at the expense of basal progenitor production.

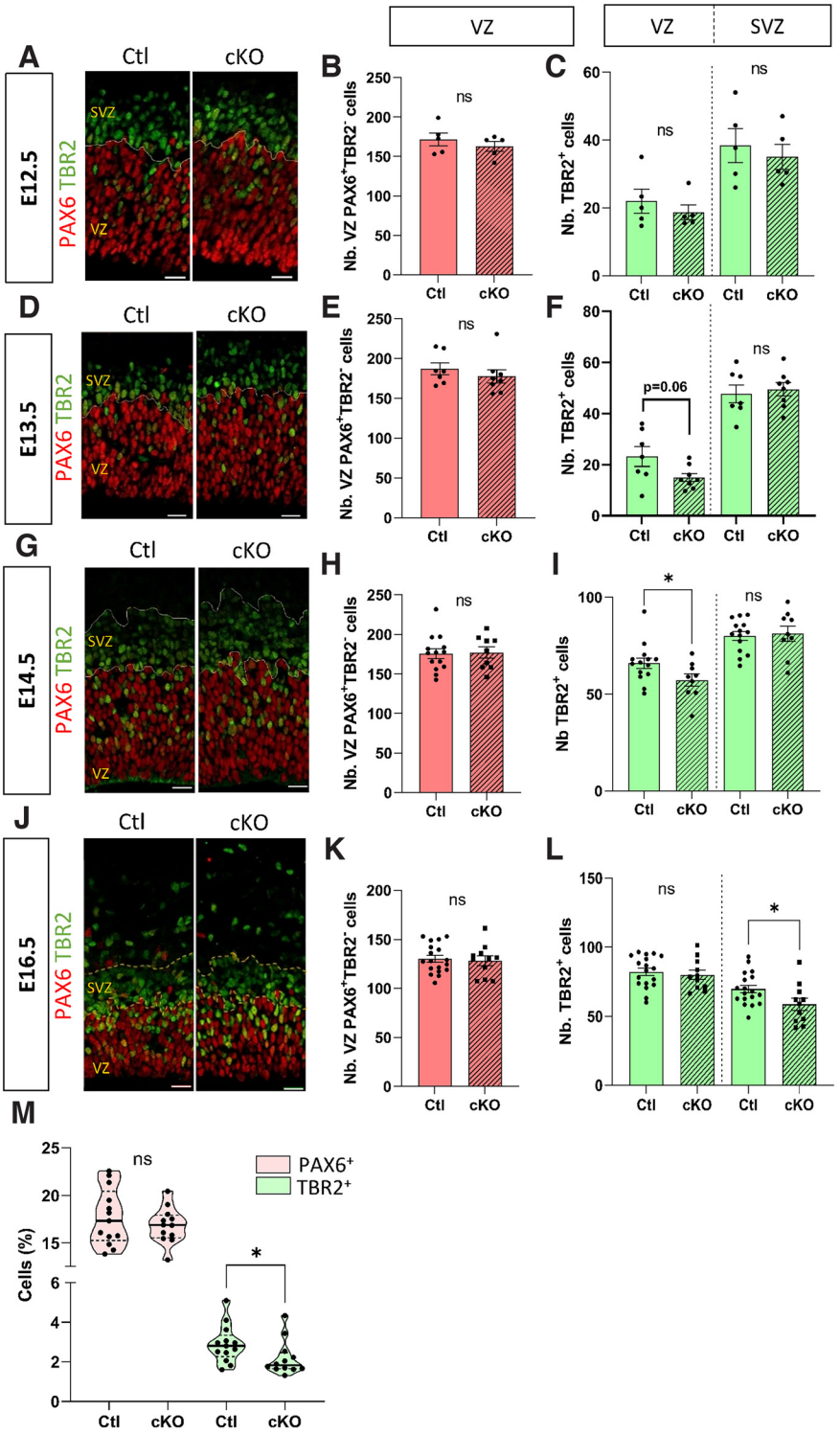

Figure 3. Cdc25b loss of function impairs basal progenitor production. ***A***, ***D***, ***G***, ***J***, PAX6 and TBR2 immunostaining on E12.5 (***A***), E13.5 (***D***), E14.5 (***G***), and E16.5 (***J***) coronal brain sections, in Ctl and cKO embryos. ***B***, ***C***, ***E***, ***F***, ***H***, ***I***, ***K***, ***L***, Quantification of PAX6$^+$ cells in the VZ (aRGs) and TBR2$^+$ cells in the VZ and SVZ (bIPs) at E12.5 (***B***,***C***), $n = 5$; E13.5 (***E***,***F***), $n = 7$ or 8; E14.5 (***H***, ***I***), $n = 9$-14, E16.5 (***K***,***L***), $n = 11$-18 in Ctl and cKO embryos. Each point is the mean value of 3 sections/embryo. Mann–Whitney *t* test and mixed model. ***I***, $^*p = 0.05$. ***L***. $^*p = 0.025$, mixed model. ***M***, Flow cytometry analysis of the proportion of PAX6 + (aRGs + bRGs) and TBR2+ (bIPs) singulates cells for Ctl and cKO E14.5 cortices. Each point represents the percentage of cells for one embryo. Ctl, $n = 13$; cKO, $n = 12$. Mann–Whitney. $^*p = 0.03$. Scale bars, 20 µm.

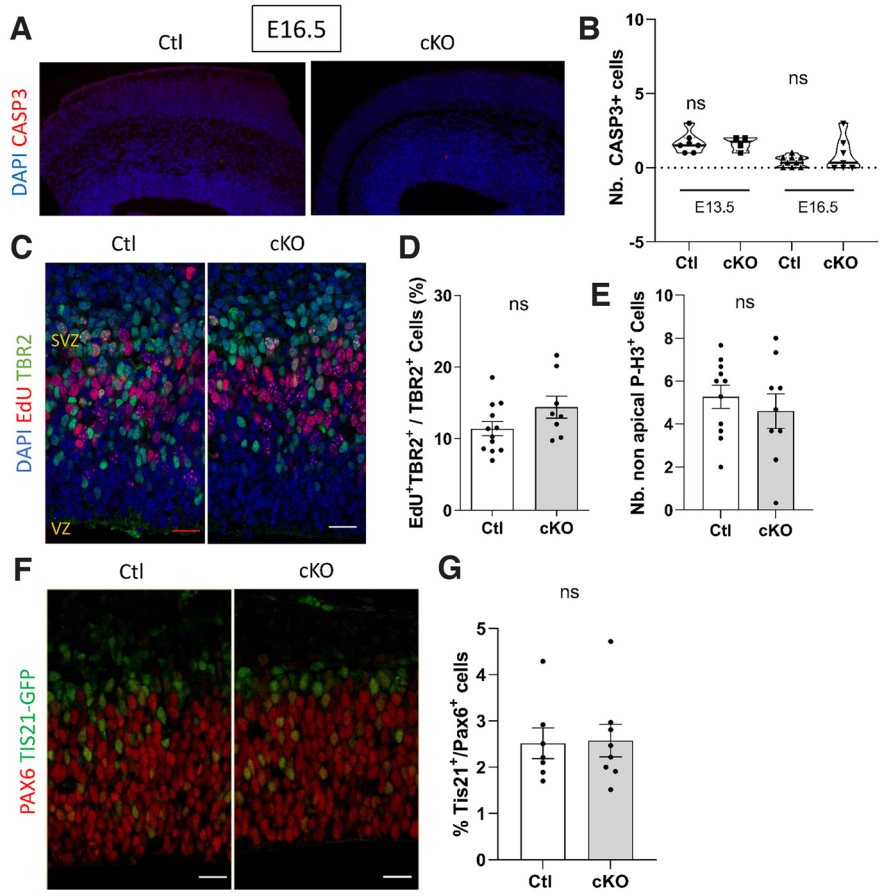

Figure 4. The reduction of bIP cells in cKOs is not because of increased cell death, reduced proliferation rate, or a change of the mode of division of aRGs. ***A***, Immunostaining of CAPS3$^+$ cells on E16.5 coronal sections. ***B***, Quantification of activated CASP3$^+$ cells on frontal brain sections of Ctl and cKO embryos at E13.5 and E16.5. Each point is the mean value of counting in 3 sections/embryo. E13.5: Ctl, $n = 7$; cKO, $n = 4$; E16.5: Ctl, $n = 9$; cKO, $n = 7$. Mann–Whitney. ***C***, Tbr2 and EdU labeling on coronal section after 1H EdU pulse just before harvesting embryos at E14.5 ***D***, Quantification of EdU$^+$ cells among total Tbr2$^+$ cells (bIPs) in Ctl and cKO embryos at E14.5. Ctl, $n = 12$; cKO, $n = 8$. Mann–Whitney. ***E***, Quantification of P-H3$^+$TBR2$^+$ cells (nonapical mitotic bIPs) in E14.5 Ctl and cKO embryos. Ctl, $n = 11$; cKO, $n = 9$. Mixed model. ***F***, PAX6 Immunostaining on brain coronal sections at E13.5 in TIS21-GFP$^+$ Ctl or cKO embryos. ***G***, Quantification of PAX6$^+$ TIS21-GFP$^+$ cells (differentiating aRGs) among PAX6$^+$ cells. Each point is the mean value of 3 sections/embryo. Mixed model. Scale bars, 20 μm.

The production of basal progenitors is impaired in cKO

To assess whether basal progenitor production is impaired in cKOs or whether the increased number of TBR1$^+$ neurons is because of premature differentiation of bIPs, we analyzed the dynamics of the production of the different progenitor types in *Cdc25b*^{cKO} embryos. We examined aRG distribution (PAX6$^+$ cells in the VZ and SVZ), bIP cell production (TBR2$^+$ newborn cells in the VZ), and bIP accumulation (TBR2$^+$ cells that have migrated in the SVZ), in the lateral part of the hemicortex between E12.5 and E16.5 (Fig. 3). The number of aRGs is not significantly affected at any of the four stages analyzed in *Cdc25b*^{cKO} embryos (Fig. 3*B*,*E*,*H*,*K*), and they are correctly located in the VZ (Fig. 3*A*,*D*,*G*,*J*). bIP production starts to be impaired from E12.5, being significantly reduced by E13.5 (Fig. 3*G*,*I*), and this decrease leads to a deficit of bIP in the SVZ at E16.5 (Fig. 3*J*,*L*). To consolidate these data, we also quantified the total number of PAX6$^+$ and TBR2$^+$ cells in control (Ctl) and *Cdc25b*^{cKO} cortices using cytometry (Jungas et al., 2020). While the total number of PAX6$^+$ cells is not modified, the number of TBR2$^+$ cells is significantly reduced in *Cdc25b*^{cKO} at E14.5, confirming that bIP but not aRG production is affected in *Cdc25b*^{cKO} (Fig. 3*M*). We verified that this reduction was not because of apoptosis, by quantifying activated Caspase3$^+$ cells in the progenitor zone at E13.5 and E16.5, and we observed no difference between Ctl and *Cdc25b*^{cKO} cortices (Fig. 4*A*,*B*). In addition, we quantified proliferation of bIPs (TBR2$^+$ cells in VZ and SVZ) at E14.5 and found that proliferative and mitotic indexes were normal, ruling out that the reduced bIP number was because of a proliferation defect in these cells (Fig. 4*C*,*D*). Together, these results indicate that the reduced number of basal progenitors in *Cdc25b*^{cKO} is most likely because of a reduction in their production from aRGs. As the number of aRGs is not modified, this suggests that, at E13.5, in the absence of CDC25B, the progeny of aRGs is changed from giving one aRG + one bIP to one aRG + one neuron. If this scenario is true, the balance between proliferative versus neurogenic division should not change in *Cdc25b*^{cKO}, as all three types of division mentioned above are neurogenic divisions. To assess this, we generated *Cdc25b*^{cKO} mice carrying a Tis21-GFP allele to distinguish aRGs committed to a neuronal or bIP fate (TIS21$^+$) from self-expanding aRGs (TIS21$^-$) (Haubensak et al., 2004; Attardo et al., 2008). We did not detect any change in the number of TIS21-GFP cells among aRGs at E13.5 in *Cdc25b*^{cKO} compared with the Ctl (Fig. 4*F*,*G*), confirming that CDC25B does not change the mode of division of aRGs from proliferative to neurogenic but rather influences the fate of neurogenic divisions.

Overall, these analyses of neuron and progenitor production at several developmental stages indicate a transient increase in neuron production, accompanied by a transient decrease in bIP production in *Cdc25b*^{cKO} embryos, with no change in aRG numbers. This suggests that in *Cdc25b*^{cKO}, aRGs transiently produce neurons instead of bIPS, and that CDC25B controls the tempo of switch between direct versus indirect neurogenesis.

The control of basal progenitor production by CDC25B requires CDK interaction

We previously showed that CDC25B can act independently of CDK interaction and G_2 phase regulation in the developing spinal cord (Bonnet et al., 2018). To test whether its role in cortical neurogenesis is dependent or independent of CDK interaction, we compared the effect of CDC25B gain of function with that of a mutated form of CDC25B, CDC25BdelCDK, which is no longer able to interact with CDK1 to regulate G_2 phase length (Bonnet et al., 2018). We used *in utero* electroporation at E13.5 and analyzed the fate of electroporated cells 28 h later (Fig. 5*A*). Compared with a GFP$^+$ control vector, overexpressing CDC25B increases the number of TBR2$^+$ cells without changing the

number of aRGs (TBR2$^-$ cells in the VZ), indicating that CDC25B is sufficient to promote bIP production (Fig. 5*B–D*). Unlike WT CDC25B, ectopic expression of CDC25BdelCDK does not alter the number of TBR2$^+$ cells (Fig. 5*B*,*C*). These results clearly show that CDC25B is sufficient to enhance bIP production and that this effect requires an interaction with CDK, suggesting that this control is exerted via a modification of the duration of the G_2 phase.

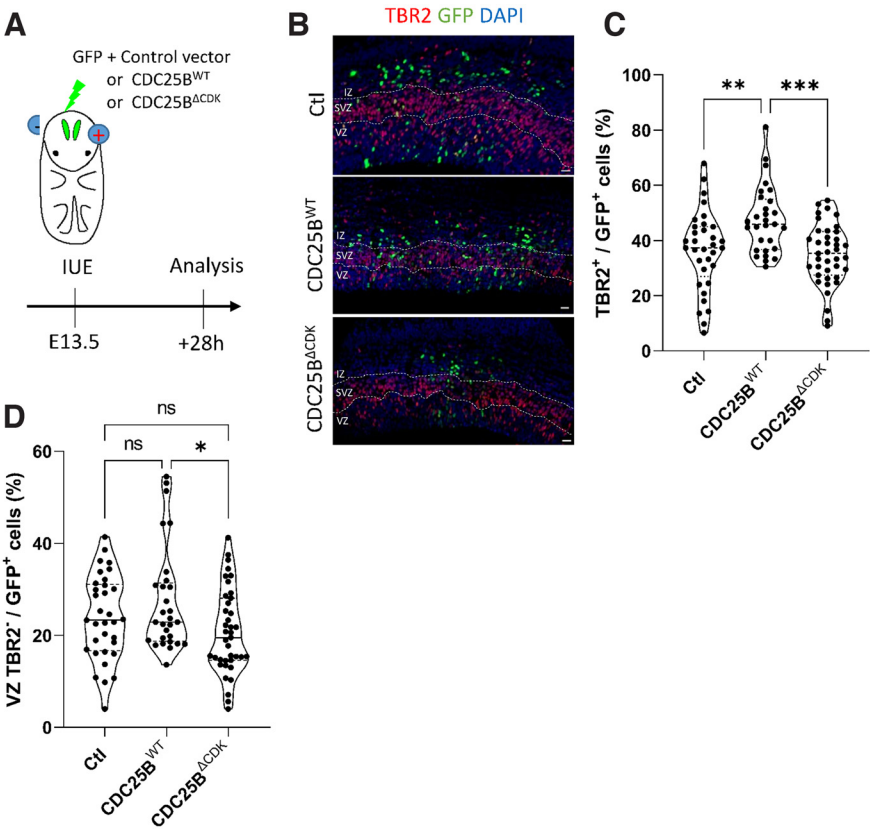

Figure 5. Cdc25b regulation of bIP production is CDK1-dependent. ***A***, Schematic representation and timeline of *in utero* electroporation experiments. ***B***, GFP and TBR2 immunostaining on E14.5 brain coronal sections after *in utero* electroporation of a pmp-LacZ (CTL), pmp-CDC25BWT (CDC25BWT), or pmp-CDC25BdelCDK (CDC25BΔCDK) expression vectors at E13.5. ***C***, Quantification of GFP$^+$ cells, which are TBR2$^+$ (bIPs) per section of CTL, CDC25BWT, or CDC25BΔCDK electroporated embryos. $^{**}p = 0.007$; $^{***}p < 0.0004$; Kruskal–Wallis. ***D***, Quantification of GFP$^+$ cells that are TBR2$^-$ in the VZ (aRGs) after electroporation Kruskal–Wallis. $^*p = 0.003$. ***C***, ***D***, Each point represents the mean value for 3 *z* sections/embryo. Ctl, $n = 33$; CDC25BWT, $n = 29$; CDC25BΔCDK, $n = 39$. IZ, Intermediate zone. Scale bars, 20 µm.

Cdc25b loss of function severely increases the length of the G_2 phase without affecting the total duration of the cell cycle

Knowing the role of CDC25B in the control of G_2/M cell cycle phase transition, and as bIP production involves CDC25B/CDK interaction, the defect in bIP production could be because of a defect in cell cycle parameters in aRGs of *Cdc25b*^{cKO} embryos. We first measured the duration of the G_2 phase using the PLM paradigm (Quastler and Sherman, 1959). Embryos were harvested 2, 3, 4 h (Fig. 6*A*) or 6 h (not shown) after EdU (5-ethynyl-2′-deoxyuridine) administration, and we quantified the percentage of P-H3$^+$(Phospho-histone 3) EdU$^+$/P-H3$^+$ with increasing exposure times to EdU (Fig. 6*A*,*B*). We found that this percentage was consistently lower in aRGs from *Cdc25b*^{cKO} embryos.

Because the progression of this percentage is proportional to the duration of the G_2 phase, we were able to extract an average length of the G_2 phase. Loss of function of *Cdc25b* in aRGs led to a significant increase in the duration of the G_2 phase at E14.5, from 2 h 12 in controls to 4 h 05 in *Cdc25b*^{cKO} already detected at E12.5 (Fig. 6*B*; Table 1). In addition, we observed a strong delay in apical migration of EdU-labeled cycling progenitors (Fig. 6*C*), resulting in a reduction in the number of apical mitosis (P-H3$^+$ cells; Fig. 6*D*), coherent with the G_2 phase lengthening. We then determined whether this lengthening of G_2 phase duration in progenitors affects their proliferation rate. We collected embryos after 1 h of EdU administration at E14.5 and quantified the EdU$^+$ cells among the aRGs (VZ, TBR2$^-$ cells; Fig. 6*E*). This percentage reflects the proportion of aRGs in S phase, and we did not observe any difference between Ctl and *Cdc25b*^{cKO} embryos (Fig. 6*E*). As the rate of proliferating cells was unaffected, we next investigated whether the lengthening of the G_2 phase caused a general slowdown of the total cell cycle length in aRGs. We performed dual EdU and BrdU labeling to estimate total cell cycle length (Tc) and S phase (TS) durations, as described by Martynoga et al. (2005). As shown in Figure 6*F*, neither the total cell cycle length nor the TS phase is significantly modified in aRGs of *Cdc25b*^{cKO} embryos. From this result, we conclude that a shortening of the G_1 phase duration may be associated to the significant lengthening of the G_2 phase. To confirm this hypothesis, we directly assessed the length of the G_1 phase by counting the number of cells expressing CCND1 (specifically expressed during the G_1 phase) among the aRGs. We observed a reduction in the number of CCND1$^+$ labeled nuclei in *Cdc25b*^{cKO} aRGs (Fig. 6*G*), indicating that the G_1 phase is shorter in these cells.

In conclusion, the removal of CDC25B in aRGs leads to a substantial lengthening of the G_2 phase (85% length increase; Table 1), as well as a shortening of the G_1, resulting in a normal cell cycle length and proliferation rate. If these length changes are considered in proportion to their average length, then the most considerable change we observed is in the duration of the G_2 phase (Table 1).

G_2 phase shortening drives an increase in bIP production

As the duration of the G_2 phase is almost doubled in *Cdc25b*^{cKO}, we next investigated whether this lengthening could play a role in controlling the rate of bIP production. To this end, we turned to cortical slice cultures and applied pharmacological treatments to modulate the duration of the G_2 phase. First, we treated cortical slices of E13.5 WT embryos with PD0166285, a Wee1/Myt1 inhibitor in conditions that do not induce toxicity (Fig. 7*A*) (Baffet et al., 2015). As Wee1 and Myt1 prevent mitosis entry through negatively regulating CDK1 activity (Potapova et al., 2009), their inhibition leads to an increase in CDK1 activity and thus to a shortening of the G_2 phase. We first determined that PD0166285 treatment at 1 µm has an effect on G_2 length in our cultures. For that, we quantified the number of EdU$^+$/P-H3$^+$

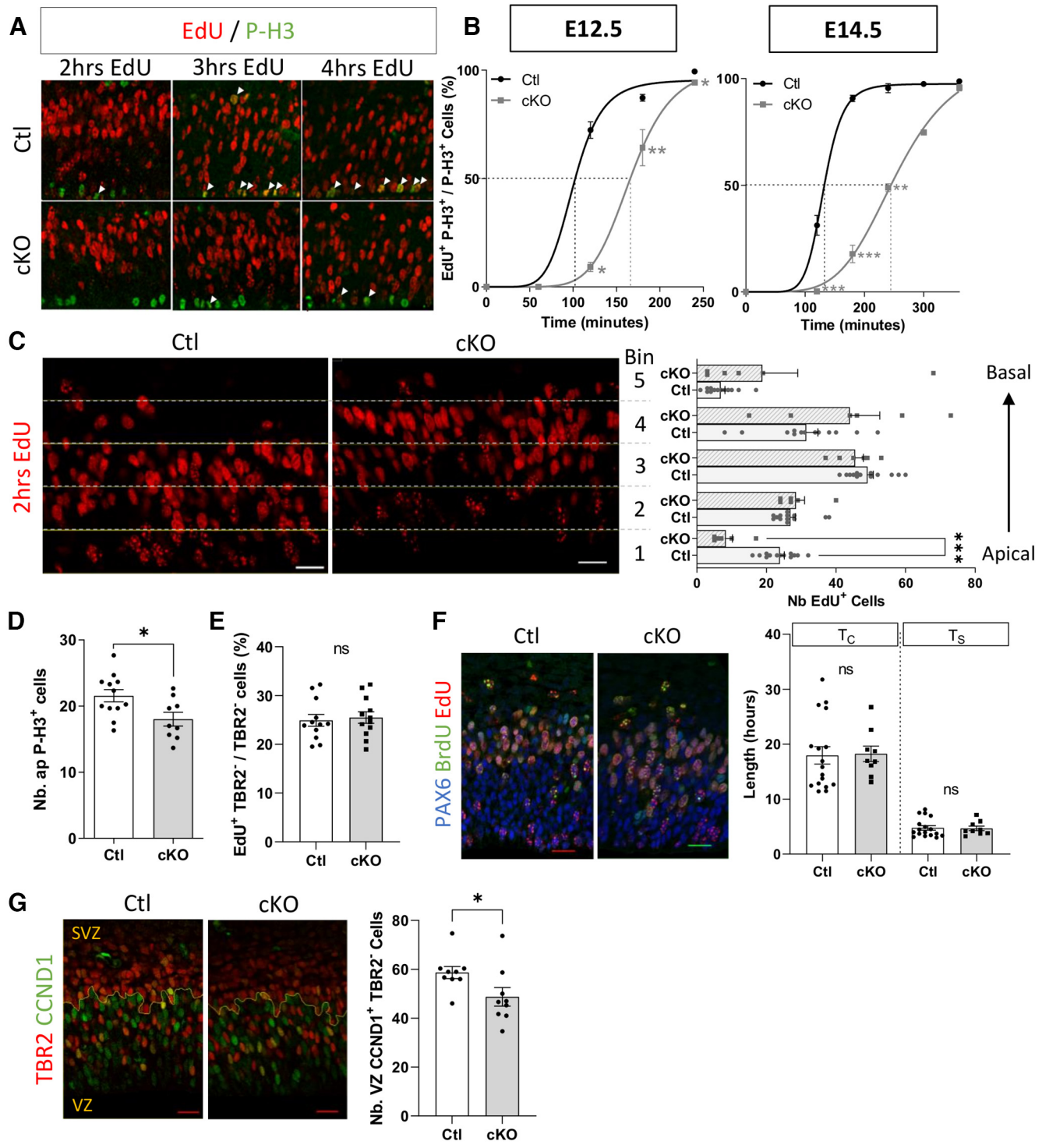

Figure 6. Cdc25b removal significantly lengthens the G_2 phase of aRG progenitors. ***A***, P-H3 labeling after 2, 3, and 4 h of EdU pulse in Ctl and cKO embryos at E14.5. ***B***, Quantification of the proportion of apical (aRG) EdU^+ $P\text{-}H3^+/P\text{-}H3^+$ cells (***A***, arrowheads). T_{G2} corresponds to the time when 50% of $P\text{-}H3^+$ cells are EdU^+ (indicated by the dotted lines). Mann–Whitney *t* test. $n = 2$-10. $^*p < 0.05$. $^{**}p < 0.01$. $^{***}p < 0.0001$. ***C***, EdU^+ cell quantification after 2 h EdU pulse, in 30 µm high bin from apical (bin 1) to basal side (bin 5), in Ctl and cKO embryos at E14.5. Mann–Whitney *t* test. $n = 6$-13. $^{***}p < 0.0001$. ***D***, Quantification of apical $P\text{-}H3^+$ cells in Ctl and cKO E14.5 cortices. Mann–Whitney and mixed model. $n = 9$-12. $^*p = 0.023$. ***E***, Quantification of EdU^+ cells among VZ $TBR2^-$ (aRGs) cells after 1 h EdU pulse in Ctl and cKO E14.5 embryos. Mixed model. $n = 12$. ***F***, EdU/BrdU double-labeling experiments to determine total cell cycle length (T_C) and S phase duration (T_S) of VZ $PAX6^+$ cells (aRG), which were calculated from counts of EdU^+BrdU^- and EdU^+BrdU^+ cells as described previously (Martynoga et al., 2005). Bar plots represent the average length of measured T_C and T_S in aRGs of Ctl and cKO E14.5 embryos. Mann–Whitney *t* test and mixed model. $n = 9$-17. ***G***, CCND1/TBR2 double immunostaining to determine the proportion of progenitor in G_1 phase. Quantification of $CCND1^+$ cells among VZ $TBR2^-$ (aRGs) cells in Ctl and cKO E14.5 cortices. Mixed model. $n = 9$. $^*p = 0.023$. In bar plots, each point is the mean value of 3 sections/embryo. Scale bars, 20 µm.

cells among the $P\text{-}H3^+$ cells, following 2 h EdU incorporation just before culture arrest. The percentage of EdU^+ cells was identical between untreated and treated controls (~22% in both conditions, not shown). This indicates that the rate of proliferation is not significantly altered by pharmacological treatment and that the cortical slices are still in good physiological state at the end of the culture. We confirmed that this treatment effectively reduces the time spent in G_2 phase by considering the percentage

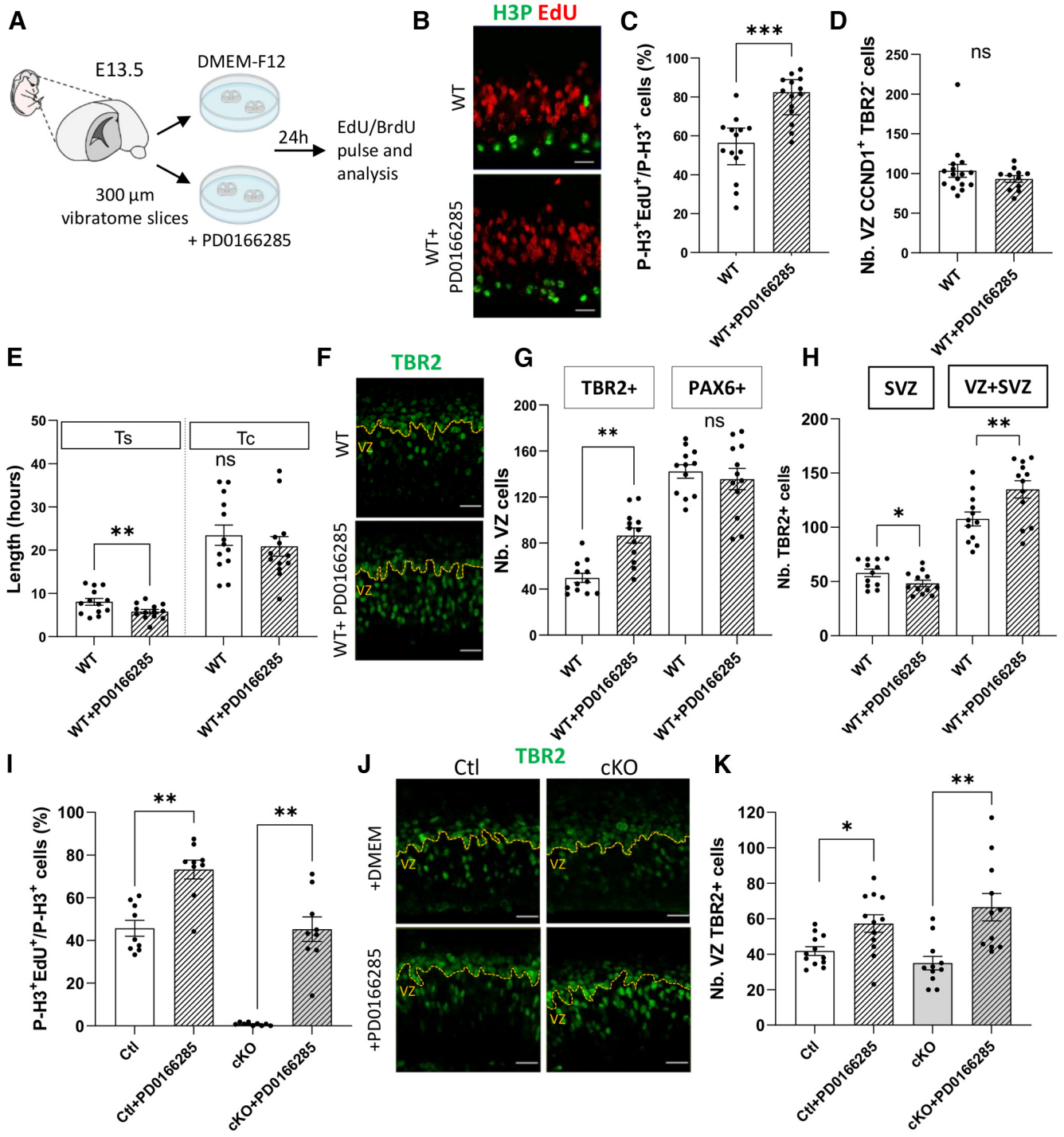

Figure 7. G_2 phase shortening triggers bIP production. ***A***, Schematic representation of embryo brain slice culture experiments. ***B***, P-H3 labeling after 2 h of EdU pulse in Ctl and cKO embryos at the end of the culture. ***C***, Percentage of $EDU^+H3P^+/H3P^+$ cells following 2 h EdU pulse, in untreated and PD0166285-treated WT brain slices. Wilcoxon test. $n = 14$. $^{***}p < 0.0001$. ***D***, Quantification of $CCND1^+$ $TBR2^-$ cells (aRG in G_1 phase) in WT and WT+PD0166285 brain slices. Wilcoxon test. $n = 11$-16. ***E***, Total cell cycle length (T_C) and S phase duration (T_S) of VZ $TBR2^-$ cells (aRGs) in WT and WT+PD0166285 brain slices. Wilcoxon test. $n = 13$. $^{**}p < 0.01$. ***F***, TBR2 immunostaining on WT and WT+PD0166285 brain slices ***G***, Quantification of bIPs ($TBR2^+$ cells) and aRGs ($TBR2^-$ cells) in the VZ of WT and WT+PD0166285 brain slices. Wilcoxon test. $n = 17$. $^{**}p < 0.01$. ***H***, Quantification of the number of $TBR2^+$ cells in the SVZ and VZ+SVZ in the same sections as in Figure 6*F*, *G* (WT and WT+PD0166285 brain slices). Wilcoxon test. $^{*}p = 0.02$. $^{**}p = 0.007$. ***I***, Percentage of $EDU^+H3P^+/H3P^+$ cells following a 2 h EdU pulse in untreated or PD0166285-treated, Ctl or cKO brain slices. Wilcoxon test. $n = 9$. $^{**}p < 0.01$. ***J***, TBR2 immunostaining on untreated or PD0166285-treated Ctl or cKO brain slices. ***K***, Quantification of $TBR2^+$ cells (bIPs) in the VZ of untreated or PD0166285-treated, Ctl or cKO brain slices. Wilcoxon test. $n = 9$. $^{*}p < 0.05$. $^{**}p < 0.01$. Each point represents the mean value of 3 sections/embryo. Scale bars, 20 µm.

of $EdU^+P\text{-}H3^+/P\text{-}H3^+$ cells in untreated and treated samples (increased 1.5× in treated cortices; Fig. 7*B*,*C*). We analyzed the impact of this treatment on the duration of the G_1 and S phases and on the total duration of the cell cycle. We found that S phase is significantly reduced by PD0166285 treatment, whereas G_1 phase duration and total cell cycle length are not significantly modified (Fig. 7*D*,*E*). We then counted the number of $TBR2^+$ cells in treated and untreated slices and observed that

pharmacological shortening of the G_2 phase leads to a doubling of the number of bIPs in the VZ (Fig. 7*F–H*), leading to a global increase of bIP cells in the progenitor zone. We then investigated whether this treatment would be sufficient to correct the defect of bIP production in *Cdc25b*^{cKO} cortices. We therefore applied the same experimental protocol as above to *Cdc25b*^{cKO} and control littermates. As observed on WT embryos, treatment with 1 μM PD0166285 leads to a marked increase in EdU$^+$P-H3$^+$/P-H3$^+$ cells in both control and *Cdc25b*^{cKO}-treated slices, indicating a shortening of the G_2 phase, with the EdU$^+$P-H3$^+$/P-H3$^+$ ratio in treated *Cdc25b*^{cKO} slices now at the level of untreated control littermates (Fig. 7*I*). We then checked the number of TBR2$^+$ cells in the VZ and observed a significant increase of these cells in treated versus untreated *Cdc25b*^{cKO} slices (1.9-fold increase) and treated versus untreated control littermates (1.5-fold increase) (Fig. 7*J*,*K*). This indicates that shortening the G_2 length in *Cdc25b*^{cKO} is sufficient to restore efficient bIP production.

Overall, these results indicate that the duration of the G_2 phase is an important parameter when controlling bIP production during early phases of cortical development.

Discussion

In this study, we investigate the function of CDC25B during corticogenesis. We show that removing CDC25B function leads to a transient increase in neuron numbers at early stages, accompanied by a decrease in the number of intermediate basal progenitors. This imbalance of neuron/progenitor number is because of a modification of the G_2 phase length in apical progenitors. We propose a model in which CDC25B expression in aRGs controls the switch from direct to indirect neurogenesis through modulation of G_2 phase length.

In the developing neocortex, neurons can be produced either directly from asymmetric division of apical progenitors or indirectly from symmetric division of intermediate basal progenitors (Govindan and Jabaudon, 2017). Controlling the balance between these two modes of production is important for the integrity and size of the cortex, but it also has an impact on the type of neurons that are produced (Haubensak et al., 2004; Attardo et al., 2008; Govindan and Jabaudon, 2017). In *Cdc25b*^{cKO}, we observe a specific increase in TBR1$^+$ neurons at E13.5, concomitant with a decrease in bIP number. Conversely, a CDC25B gain of function at E13.5 leads to an increase in bIPs in the VZ. We can exclude that the increase in neuron production is because of an increase in aRG production, as the number of aRG is not altered in *Cdc25b*^{cKO}. Furthermore, if this scenario were true, one would expect that there would also be more bIPs produced. This alteration in the number of bIPs and neurons is also not because of an overproduction of neurons from bIPs. Indeed, the increase in neuron production in *Cdc25b*^{cKO} embryos precedes the decrease in bIPs of the SVZ; and if bIPs differentiated into neurons prematurely, we should detect a decrease in bIP cells in the SVZ as early as E13.5, which is not the case. Since the number of aRGs is normal and the ratio of proliferative to neurogenic division is unchanged in *Cdc25b*^{cKO}, our results indicate a change in the progeny of asymmetrically dividing aRGs, producing neurons instead of bIPs (Fig. 8). This phenotype is transient, as at E16.5 we no longer observe a defect in bIP number in the VZ, and the total number of neurons is unchanged in *Cdc25b*^{cKO}. This could indicate either a compensation mechanism (Freret-Hodara et al., 2017) or, alternatively, that CDC25B is only required during early

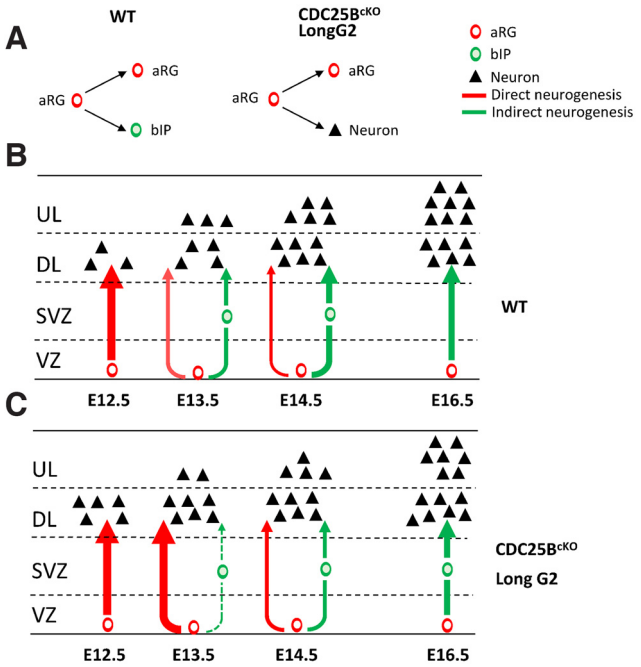

Figure 8. Model for CDC25B function during cortical neurogenesis. ***A***, In CDC25B^{cKO}, apical progenitor asymmetric divisions produce a neuron instead of a basal progenitor. ***B***, In a normal situation, deep layer neurons are produced mainly between E12.5 and E13.5, directly from APs (direct neurogenesis). At E13.5, the production of bIPs begins in the VZ, which later divides in the SVZ to give rise to neurons (indirect neurogenesis). Indirect neurogenesis gradually becomes the main mechanism of neuron production. ***C***, In CDC25B^{cKO}, the ratio between direct and indirect neurogenesis is disturbed. Direct neurogenesis is maintained for a longer period of time, leading to an early production of deep layer neurons at the expense of bIP production. This imbalance is progressively compensated to reach normal neuronal production around E16.5. Because of this delay in the direct to indirect neurogenesis switch, upper layer neuron number is slightly reduced at P0.

corticogenesis stages, at the time of the direct to indirect neurogenesis switch. Hence, we propose that, in *Cdc25b*^{cKO}, the switch from direct to indirect neurogenesis is delayed, leading to a bIP/neuron production imbalance that is progressively compensated for (Fig. 8). This delay and the resulting decrease in the number of TBR2$^+$ progenitors lead to a slight reduction of the CUX1$^+$ upper layer neuron number at birth. This is consistent with the fact that these neurons are mainly produced from TBR2$^+$ bIPs (Vasistha et al., 2015).

In a previous study, we have shown that, in the developing spinal cord, CDC25B promotes progenitor maturation as it increases the number of progenitors performing neurogenic divisions at the expense of those that self-renew (Bonnet et al., 2018). Other studies have also made indirect links between defects in the balance between proliferative versus neurogenic division during cortical neurogenesis and CDC25B misregulation (Gruber et al., 2011; Wu et al., 2014). We did not see any change in the proliferative versus neurogenic mode of division in CDC25B mutant cortices. Our previous observations made in the chicken neural tube indicate that part of CDC25B function during neurogenesis is independent of its function on the cell cycle (Bonnet et al., 2018). In the neocortex, the phenotype we describe requires interaction with CDK1; but in both tissues, CDC25B promotes progenitor maturation.

Another important result is that this neurogenesis defect is linked to a significant modification of the G_2 phase length. First, in *Cdc25b*^{cKO}, the most important change in cell cycle parameters in aRGs is a substantial lengthening of the G_2 length. Second, the

CDC25BdelCDK gain of function that cannot regulate G_2 phase length (Bonnet et al., 2018) does not phenocopy the WT form of CDC25B that increases bIP production, indicating that the defect in bIP production is directly related to the ability of CDC25B to regulate CDK1 activity. Third, we provide evidence that shortening the G_2 phase in WT embryos using a pharmacological treatment is sufficient to stimulate bIP production. Fourth, this treatment is sufficient to restore an efficient bIP production in *Cdc25b*^{cKO}. In these experiments, either the G_1 phase length or the S phase length was slightly reduced. However, the changes in these phases are well below the levels that have been described as leading to alterations in aRG progenitor mode of division and fate (Lange et al., 2009; Pilaz et al., 2009; Arai et al., 2011) . Furthermore, the only parameter that varies dramatically and significantly in both *Cdc25b*^{cKO} and PD0166285 treatment is the length of the G_2 phase. This argues for a role of G_2 phase duration, rather than a role of duration in these experimental conditions. In *Cdc25b*^{cKO}, the G_2 lengthening is associated with a perturbation of the apical nuclear migration, as $BrdU^+$ aRGs nuclei take more time to reach the apical surface to perform mitosis. This perturbation is likely because apical migration and G_2 phase processing are linked, and cell cycle progression is a prerequisite to normal apical migration (Ueno et al., 2006; Baffet et al., 2015).

What is the relevance of this finding concerning the link between G_2 phase length and bIP production in a normal context? Most studies in which GAP phase length has been measured indicate that, while G_1 phase length increases during tissue maturation, G_2 phase length appears to be more stable, ~2 h in aRGs and bIPs, and does not change significantly during embryonic cortex maturation (Pilaz et al., 2009; Arai et al., 2011; Hasenpusch-Theil et al., 2018). However, these studies were performed at the level of cell population, which could have masked some heterogeneity in the duration of the G_2 phase between different progenitors. Live imaging analysis performed in the developing spinal cord indicates that the length of G_2 phase is more heterogeneous than previously described, ranging from 40 to 175 min (Molina et al., 2022). In the developing neocortex, data provided using real-time analysis of proliferating cell nuclear antigen-expressing apical progenitors show that the proportion of aRGs in G_2 phase varies between E12 and E16 (Fousse et al., 2019). A recent study from Hagey et al. (2020) also emphasizes that cortical progenitors are not equivalent regarding G_2/M phase length. Indeed, by performing single-cell RNA-Seq at different stages (from E9.5 to E18.5), they identify two temporally distinct cortical differentiation trajectories. At E11.5, progenitors can be separated into two groups: one group of lineage-committed progenitors, giving rise to deep layer neurons; and one group of uncommitted multipotent aRGs that will give rise to later born lineages. The group of lineage-committed progenitors spends more time in G_1 and expresses G_1-associated cyclin, whereas the uncommitted ones are more prone to be found in G_2/M and express high levels of M phase associated genes, including CDK1. Interestingly, *Cdc25B* is found among the overrepresented genes in the upper layer path, compared with the deep layer 1 (Hagey et al., 2020, their supplementary data 5) (*Cdc25B* in upper-layer trajectory gene sets, p-adjust = 4.04E-15). Moreover, data mining (Telley et al., 2019; Hagey et al., 2020) indicates that *Cdc25B* transcripts have the same spatial and temporal profile than genes specifically expressed in the uncommitted E11.5 aRGs (not shown). Hence, CDC25B activity, by accelerating mitosis entry, could contribute to the maintenance of the uncommitted progenitor pool at early stages, to ensure correct production of upper layer neurons later on. Different G_2 length duration, by changing the exposure time to instructive signaling pathways such as the Slit-Robo and/or the Notch signaling pathways (Murciano et al., 2002; Cárdenas et al., 2018; Fousse et al., 2019; Hagey et al., 2020), could lead to different fate decisions after mitosis.

In conclusion, our study sheds light on a new role for CDC25B and G_2 phase length in controlling the fate of apical progenitors during early steps of corticogenesis, thereby controlling the switch from direct to indirect neuronal differentiation. The apparition of indirect neurogenesis is considered a milestone of mammalian cortical evolution leading to cortical expansion (Borrell, 2019). Expression of CDC25B in aRGs, by favoring bIP production, would be a way of supporting this evolutive trait. Future investigation will be necessary to understand the molecular mechanisms that support this function.

References

Agathocleous M, Locker M, Harris WA, Perron M (2007) A general role of hedgehog in the regulation of proliferation. Cell Cycle 6:156–159.

Agius E, Bel-Vialar S, Bonnet F, Pituello F (2015) Cell cycle and cell fate in the developing nervous system: the role of CDC25B phosphatase. Cell Tissue Res 359:201–213.

Arai Y, Pulvers JN, Haffner C, Schilling B, Nusslein I, Calegari F, Huttner WB (2011) Neural stem and progenitor cells shorten S phase on commitment to neuron production. Nat Commun 2:154.

Attardo A, Calegari F, Haubensak W, Wilsch-Brauninger M, Huttner WB (2008) Live imaging at the onset of cortical neurogenesis reveals differential appearance of the neuronal phenotype in apical versus basal progenitor progeny. PLoS One 3:e2388.

Baffet AD, Hu DJ, Vallee RB (2015) Cdk1 activates pre-mitotic nuclear envelope dynein recruitment and apical nuclear migration in neural stem cells. Dev Cell 33:703–716.

Barbelanne M, Tsang WY (2014) Molecular and cellular basis of autosomal recessive primary microcephaly. Biomed Res Int 2014:547986.

Benazeraf B, Chen Q, Peco E, Lobjois V, Medevielle F, Ducommun B, Pituello F (2006) Identification of an unexpected link between the Shh pathway and a G_2/M regulator, the phosphatase CDC25B. Dev Biol 294:133–147.

Bonnet F, Molina A, Roussat M, Azais M, Vialar S, Gautrais J, Pituello F, Agius E (2018) Neurogenic decisions require a cell cycle independent function of the CDC25B phosphatase. Elife 7:e32937.

Borrell V (2019) Recent advances in understanding neocortical development. F1000Res 8:1791.

Boutros R, Ducommun B (2008) Asymmetric localization of the CDC25B phosphatase to the mother centrosome during interphase. Cell Cycle 7:401–406.

Boutros R, Lobjois V, Ducommun B (2007) CDC25B involvement in the centrosome duplication cycle and in microtubule nucleation. Cancer Res 67:11557–11564.

Boutros R, Lorenzo C, Mondesert O, Jauneau A, Oakes V, Dozier C, Gabrielli B, Ducommun B (2011) CDC25B associates with a centrin 2-containing complex and is involved in maintaining centrosome integrity. Biol Cell 103:55–68.

Boutros R, Mondesert O, Lorenzo C, Astuti P, McArthur G, Chircop M, Ducommun B, Gabrielli B (2013) CDC25B overexpression stabilises centrin 2 and promotes the formation of excess centriolar foci. PLoS One 8: e67822.

Cárdenas A, Villalba A, de Juan Romero C, Picó E, Kyrousi C, Tzika AC, Tessier-Lavigne M, Ma L, Drukker M, Cappello S, Borrell V (2018) Evolution of cortical neurogenesis in amniotes controlled by Robo signaling levels. Cell 174:590–606.e21.

Dehay C, Kennedy H (2007) Cell-cycle control and cortical development. Nat Rev Neurosci 8:438–450.

Fawal MA, Jungas T, Kischel A, Audouard C, Iacovoni JS, Davy A (2018) Cross talk between one-carbon metabolism, Eph signaling, and histone methylation promotes neural stem cell differentiation. Cell Rep 23:2864–2873.e7.

Florio M, Albert M, Taverna E, Namba T, Brandl H, Lewitus E, Haffner C, Sykes A, Wong FK, Peters J, Guhr E, Klemroth S, Prüfer K, Kelso J,

Naumann R, Nüsslein I, Dahl A, Lachmann R, Pääbo S, Huttner WB (2015) Human-specific gene ARHGAP11B promotes basal progenitor amplification and neocortex expansion. Science 347:1465–1470.

Fousse J, Gautier E, Patti D, Dehay C (2019) Developmental changes in interkinetic nuclear migration dynamics with respect to cell-cycle progression in the mouse cerebral cortex ventricular zone. J Comp Neurol 527:1545–1557.

Freret-Hodara B, Cui Y, Griveau A, Vigier L, Arai Y, Touboul J, Pierani A (2017) Enhanced Abventricular Proliferation Compensates Cell Death in the Embryonic Cerebral Cortex. Cereb Cortex 27:4701–4718.

Gonzales KA, Liang H (2015) Transcriptomic profiling of human embryonic stem cells upon cell cycle manipulation during pluripotent state dissolution. Genom Data 6:118–119.

Gonzales KA, Liang H, Lim YS, Chan YS, Yeo JC, Tan CP, Gao B, Le B, Tan ZY, Low KY, Liou YC, Bard F, Ng HH (2015) Deterministic restriction on pluripotent state dissolution by cell-cycle pathways. Cell 162:564–579.

Govindan S, Jabaudon D (2017) Coupling progenitor and neuronal diversity in the developing neocortex. FEBS Lett 591:3960–3977.

Gruber R, Zhou Z, Sukchev M, Joerss T, Frappart PO, Wang ZQ (2011) MCPH1 regulates the neuroprogenitor division mode by coupling the centrosomal cycle with mitotic entry through the Chk1-Cdc25 pathway. Nat Cell Biol 13:1325–1334.

Hagey DW, Topcic D, Kee N, Reynaud F, Bergsland M, Perlmann T, Muhr J (2020) CYCLIN-B1/2 and -D1 act in opposition to coordinate cortical progenitor self-renewal and lineage commitment. Nat Commun 11:2898.

Hasenpusch-Theil K, West S, Kelman A, Kozic Z, Horrocks S, McMahon AP, Price DJ, Mason JO, Theil T (2018) Gli3 controls the onset of cortical neurogenesis by regulating the radial glial cell cycle through. Development 145:dev163147.

Haubensak W, Attardo A, Denk W, Huttner WB (2004) Neurons arise in the basal neuroepithelium of the early mammalian telencephalon: a major site of neurogenesis. Proc Natl Acad Sci USA 101:3196–3201.

Jungas T, Joseph M, Fawal MA, Davy A (2020) Population dynamics and neuronal polyploidy in the developing neocortex. Cereb Cortex Commun 1:tgaa063.

Kawaguchi A (2019) Temporal patterning of neocortical progenitor cells: how do they know the right time? Neurosci Res 138:3–11.

Körner K, Jerôme V, Schmidt T, Müller R (2001) Cell cycle regulation of the murine cdc25B promoter: essential role for nuclear factor-Y and a proximal repressor element. J Biol Chem 276:9662–9669.

Lange C, Huttner WB, Calegari F (2009) Cdk4/cyclinD1 overexpression in neural stem cells shortens G_1, delays neurogenesis, and promotes the generation and expansion of basal progenitors. Cell Stem Cell 5:320–331.

Locker M, Agathocleous M, Amato MA, Parain K, Harris WA, Perron M (2006) Hedgehog signaling and the retina: insights into the mechanisms controlling the proliferative properties of neural precursors. Genes Dev 20:3036–3048.

Madisen L, Zwingman TA, Sunkin SM, Oh SW, Zariwala HA, Gu H, Ng LL, Palmiter RD, Hawrylycz MJ, Jones AR, Lein ES, Zeng H (2010) A robust and high-throughput Cre reporting and characterization system for the whole mouse brain. Nat Neurosci 13:133–140.

Martynoga B, Morrison H, Price DJ, Mason JO (2005) Foxg1 is required for specification of ventral telencephalon and region-specific regulation of dorsal telencephalic precursor proliferation and apoptosis. Dev Biol 283:113–127.

Molina A, Bonnet F, Pignolet J, Lobjois V, Bel-Vialar S, Gautrais J, Pituello F, Agius E (2022) Single-cell imaging of the cell cycle reveals CDC25B-induced heterogeneity of G_1 phase length in neural progenitor cells. Development 149:dev199660.

Molyneaux BJ, Arlotta P, Menezes JR, Macklis JD (2007) Neuronal subtype specification in the cerebral cortex. Nat Rev Neurosci 8:427–437.

Murciano A, Zamora J, López-Sánchez J, Frade JM (2002) Interkinetic nuclear movement may provide spatial clues to the regulation of neurogenesis. Mol Cell Neurosci 21:285–300.

Namba T, Huttner WB (2017) Neural progenitor cells and their role in the development and evolutionary expansion of the neocortex. Wiley Interdiscip Rev Dev Biol 6:1.

Ostrem B, Lullo ED, Kriegstein A (2017) oRGs and mitotic somal translocation: a role in development and disease. Curr Opin Neurobiol 42:61–67.

Peco E, Escude T, Agius E, Sabado V, Medevielle F, Ducommun B, Pituello F (2012) The CDC25B phosphatase shortens the G_2 phase of neural progenitors and promotes efficient neuron production. Development 139:1095–1104.

Pilaz LJ, Patti D, Marcy G, Ollier E, Pfister S, Douglas RJ, Betizeau M, Gautier E, Cortay V, Doerflinger N, Kennedy H, Dehay C (2009) Forced G_1 phase reduction alters mode of division, neuron number, and laminar phenotype in the cerebral cortex. Proc Natl Acad Sci USA 106:21924–21929.

Pilaz LJ, McMahon JJ, Miller EE, Lennox AL, Suzuki A, Salmon E, Silver DL (2016) Prolonged mitosis of neural progenitors alters cell fate in the developing brain. Neuron 89:83–99.

Potapova TA, Daum JR, Byrd KS, Gorbsky GJ (2009) Fine tuning the cell cycle: activation of the Cdk1 inhibitory phosphorylation pathway during mitotic exit. Mol Biol Cell 20:1737–1748.

Quastler H, Sherman FG (1959) Cell population kinetics in the intestinal epithelium of the mouse. Exp Cell Res 17:420–438.

Telley L, Agirman G, Prados J, Amberg N, Fièvre S, Oberst P, Bartolini G, Vitali I, Cadilhac C, Hippenmeyer S, Nguyen L, Dayer A, Jabaudon D (2019) Temporal patterning of apical progenitors and their daughter neurons in the developing neocortex. Science 364:eaav2522.

Tronche F, Kellendonk C, Kretz O, Gass P, Anlag K, Orban PC, Bock R, Klein R, Schütz G (1999) Disruption of the glucocorticoid receptor gene in the nervous system results in reduced anxiety. Nat Genet 23:99–103.

Ueno M, Katayama K, Yamauchi H, Nakayama H, Doi K (2006) Cell cycle progression is required for nuclear migration of neural progenitor cells. Brain Res 1088:57–67.

Vasistha NA, García-Moreno F, Arora S, Cheung AF, Arnold SJ, Robertson EJ, Molnár Z (2015) Cortical and clonal contribution of Tbr2 expressing progenitors in the developing mouse brain. Cereb Cortex 25:3290–3302.

Wilsch-Bräuninger M, Florio M, Huttner WB (2016) Neocortex expansion in development and evolution: from cell biology to single genes. Curr Opin Neurobiol 39:122–132.

Wu X, Gu X, Han X, Du A, Jiang Y, Zhang X, Wang Y, Cao G, Zhao C (2014) A novel function for Foxm1 in interkinetic nuclear migration in the developing telencephalon and anxiety-related behavior. J Neurosci 34:1510–1522.